https://doi.org/10.1016/j.geotexmem.2023.05.003

Recycling dredged mud slurry using vacuum-solidification combined method with sustainable alkali-activated binder

By

Ding-Bao SONG[1,2], Wen-Bo CHEN[1,2*], Zhen-Yu YIN[2], Xiu-Song SHI[3], Jian-Hua YIN[2]

[1]College of Civil and Transportation Engineering, Shenzhen University, Shenzhen, China

[2]Department of Civil and Environmental Engineering, The Hong Kong Polytechnic University, Hong Kong, China.

[3]Key Lab of Ministry of Education for Geomechanics and Embankment Engineering, Hohai University, Nanjing, China

Corresponding author: Wen-Bo Chen, Email: geocwb@gmail; wb.chen@polyu.edu.hk

Abstract: Dredged sediments with high water content is difficult to be treated and beneficially reused because of their poor engineering characteristics. To treat those slurry, this paper introduces a novel mechanical-chemical combined method, i.e., vacuum-solidification (VS) combined method, and investigates its performance in dewatering and strength improvement. Corresponding model tests using vacuum-only preloading method and binder-only solidification method, respectively, were conducted. Ground granulated blast-furnace slag, an industrial by-product, activated by hydrated lime, magnesium oxide or carbide slag was used as the binder in the proposed method. The mass of discharged water due to vacuum consolidation was measured during the model test. Soil samples were taken after vacuum preloading for unconfined compression test, permeability test, X-ray diffraction, scanning electron microscopy and mercury intrusion porosimetry to analyze the strength development, hydraulic and microstructural properties of the treated soil. The results indicate that, in comparison to traditional treatment methods, the VS combined method exhibits a remarkable enhancement in both volume reduction efficiency and the strength improvement effectiveness. The type and content of activators have an obvious influence on the performance of the combined method. This study preliminarily revealed the mechanism and effect of using the VS combined method with alkali-activated GGBS as binder to treat high water content dredged mud.

Keywords: dredged sediments; mechanical properties; microstructure; alkali-activated GGBS; vacuum preloading; model test

1 Introduction

In coastal areas, the seabed is often covered with thick layers of sediment. As an example, the geological cross-section of the Hong Kong International Airport site in Fig. 1 presents a typical distribution of marine sediment layer with an average thickness of 10-15 m. The thickness of the sediment layers increases gradually with time. The particles of these sediment layers are mainly originated from soils and rocks and are transported by rivers from the land to the sea. In order to maintain the marine ecological environment and offshore engineering construction, dredging is frequently carried out to remove part of the sediments. A considerable quantity of dredged mud with high water content is produced during the dredging process (Tang et al., 2020). Additionally, the maintenance of navigation channels including rivers, lakes, reservoirs, ponds and ports also generates large amounts of dredged mud (Snellings et al., 2016; Chen et al., 2019). In China, billions of cubic meters of mud slurry are produced from various dredging projects and coastal areas each year (Huang et al., 2011; Tang et al., 2020), which poses a massive disposal problem. The poor engineering properties of dredged mud slurries, e.g. high compressibility, low permeability and negligible bearing capacity (Umehara and Zen, 1982; Yan and Ma, 2010; Xu et al., 2015; Ngo et al., 2020), exacerbate the difficulties in transporting, storing and treating these mud slurries.

The most typical way to dispose of dredged mud is to stack it in a massive storage yard (Staniszewska and Boniecja, 2017), which usually requires a long turnover period, thereby wasting land resources and potentially causing secondary environmental pollution (Svensson et al., 2022). It is vital to find a solution to quickly and efficiently deal with vast quantities of mud

slurry at high water content. Besides, the construction of infrastructure in civil engineering requires a large amount of competent fill materials, such as sand and crushed rock, while both the sustainable development strategy and shortage of natural resources impose restrictions on the exploitation of natural resources (Correia et al., 2016). Therefore, extensive studies (Siham et al., 2008; Chai et al., 2017; Feng et al., 2017; Rakshith and Singh, 2017; Wang et al., 2017; Mymrin et al., 2021) have been conducted on turning dredged mud slurry into competent fill materials in civil engineering to realize the add-value recycling of dredged materials and solve the shortage of construction fill materials at the same time, thus achieving a win-win situation in a way of high economic and social benefits.

Vacuum preloading method is a widely used mechanical dewatering and ground improvement technique for treating soft soils because of its ease of construction, low cost and good performance in strength improvement (Chai et al., 2006; Sun et al., 2018; Wang et al., 2019; Li et al., 2021; de Lillis et al., 2022). The prefabricated vertical drain (PVD) is currently used as the drainage channel in traditional vacuum preloading methods. However, using PVD to treat mud slurry with high water content has the following drawbacks: firstly, since the mud slurry with high water content has almost zero bearing capacity, it is difficult for PVD installation equipment and personnel to enter the site directly. Therefore, time-consuming and expensive pre-treatment, such as natural drying or solidification, etc., need to be carried out before the installation of PVD (Chu et al., 2012); secondly, the large settlement of the highly compressible mud slurry during the consolidation frequently leads to the significant bending of PVD, which greatly compromises the ability of the PVD to transmit vacuum pressure (Cai et al., 2017); thirdly,

the vacuum pressure in PVD significantly decreases with increasing depth, which is detrimental to improve deep soil layers (Chen et al., 2019). To treat the high-water-content dredged mud slurry, Chiba et al. (1992) suggested using a prefabricated horizontal drain (PHD) -based vacuum preloading approach. Meanwhile, the feasibility of PHD-based vacuum preloading method has been verified by a practical project in Japan. Using PHD as the drainage channel, compared with PVD, can avoid the aforementioned disadvantages of PVD, while improving the treatment efficacy of vacuum preloading (Shinsha and Kumagai, 2014; Song et al. 2023).

Another common method for the improvement of dredged materials is the chemical modification method using binder materials such as lime or cement (Sato and Kato, 2002; Zhu et al., 2007; Wang et al., 2018; Wu et al., 2019; Ho et al., 2020; Lei et al., 2020; Yoobanpot et al., 2020; Ho et al., 2021). The strength of dredged mud slurry can be quickly improved by the solidification method, but the strength improvement efficacy of this method is particularly sensitive to the initial water content of the mud slurry, with a significant drop in strength as the water content of mud slurry increases (Miura et al., 2001; Zhang et al., 2013; Sun et al., 2023). As reported by Zhang et al. (2020), with a cement amount of 30% (the weight ratio of cement to dry soil), the undrained shear strength of the stabilized mud with an initial water content of 160% was approximately 85 kPa after 28 days curing. However, when the initial water content of the mud slurry increased to 320% and 450%, respectively, the corresponding shear strength decreased substantially to 18 kPa and 5 kPa. In other words, increasing the water content of the mud slurry by 2 and 2.8 times reduced the strength of the stabilized mud slurry by up to 79% and 94%, respectively. Furthermore, cement is frequently used as a binder in current stabilization projects,

and cement production is an energy-intensive and polluting process (Chen et al., 2010). According to the reports, one tone of cement clinker requires approximately 1.5 tons of nonrenewable resources such as clay and lime, consumes 5000 MJ of energy, and produces approximately 0.9 tons of CO_2 (Anand et al., 2006; Wu et al., 2022). The cement industry is reported to be responsible for 8% of the total global CO_2 emissions from human activities worldwide (Proaño et al., 2020). Excessive usage of cement is incompatible with the sustainable development strategy. To lessen the environmental impact of the cement industry, alkali-activated slag using industrial by-products/wastes has been investigated as an alternative binder in soft soil stabilization, thanks to its comparable stabilization performance and negligible carbon footprint (Pacheco-Torgal et al., 2008; Haha et al., 2011; Yi et al., 2014; Gonzalez et al., 2021). The alkali-activated slag binder is composed of slag and alkaline activator (auxiliary component). As reported by Yi et al. (2014; 2015), hydrated lime, MgO and carbide slag (CS, a type of industrial by-product) can be served as an effective activator for ground granulated blast-furnace (GGBS). At the moment, alkali-activated slag is generally used for the stabilization of soft soil with low water content, while little research has been done to verify the strength improvement performance of mud slurry with high water content.

As for the vacuum preloading method, the maximum vacuum pressure of the preloading technique is capped at the atmospheric pressure in theory, and the vacuum pressure recorded in sites is typically lower than 90 kPa (Shinsha and Kumagai, 2014), which means there is a clear upper limit for the final stabilization performance of the vacuum preloading method. Furthermore, the high content of fines in mud slurry easily leads to clogging of band drains (i.e., PVD or PHD)

and hence reduces the efficiency of vacuum dewatering and strength improvement (Deng et al., 2019). On the other hand, if only the solidification method is used to strengthen the mud slurry, a large amount of binder must be added (Horpibulsuk et al., 2005), which is often prohibitively expensive and environmentally unfriendly. In response to the aforementioned limitations of two individual methods, mechanical-chemical combined method for treating mud at high water content was introduced (Wang et al., 2017; Lei et al., 2019; Zhang et al., 2022). The fundamental mechanism of the combined method is to modify the mud slurry by the synergistic of chemical agents and mechanical dewatering to improve the strength development. The feasibility and effectiveness of combined methods were also well evidenced by model tests (Wang et al., 2017; Lei et al., 2019; Zhang et al., 2022). However, most of the previous studies adopt PVD as drainage channel and use cement as chemical agent. Considering the disadvantages of using PVD and/or cement in treating high-water-content mud slurry, a combined technique of vacuum preloading and solidification based on PHD and alkali-activated slag, i.e., vacuum-solidification (VS) combined method, is presented in detail in this study.

Fig. 2 illustrates the implementation process of the VS combined method. First, install a layer of PHD at the bottom of the site, blow the well-mixed mud slurry and binder into the site, and then apply vacuum via the PHD layer for dewatering. Then, place a new layer of PHD on top of the first layer of mud slurry-binder mixture, followed by the blow-filling of the next layer of mixture and vacuum dewatering. Blow-filling and placing new PHD layer are performed alternatively. This method adopts PHD instead of PVD to overcome several major problems, including inaccessibility of the equipment and personnel for installation of PVD, bending of the

PVD during the consolidation process and the reduction of vacuum pressure along with soil depth. Blow-filling and vacuum dewatering are carried out simultaneously, resulting in an early involvement of vacuum dewatering and higher treatment efficiency. The binder plays a further reinforcing role in the mud treated by vacuum dewatering, reducing the amount of binder used, while enhancing the treatment effect. And the use of industrial by-product-based alkali-activated slag instead of cement as binder is more in line with sustainable development.

The main objective of this paper is to investigate the feasibility and effectiveness of the VS combined method using alkali-activated GGBS as binder to treat mud slurry with high water content and to compare the improvement performance with vacuum-only preloading (VP) method and binder-only solidification (BS) method. Three different activators, including hydrated lime, MgO and carbide slag (CS), were used for the binder of alkali-activated GGBS. The influence of the type and dosage of activator on the improvement effectiveness of VS combined method was also analyzed. The vacuum dewatering efficiency was monitored during the vacuum preloading, after which the stabilized soil samples were taken for a range of characterization tests, including unconfined compression (UC) test, permeability test, X-ray diffraction (XRD), scanning electron microscopy (SEM) and mercury intrusion porosimetry (MIP) to reveal the strength development, hydraulic and microstructure properties of stabilized soils.

2 Materials and testing scheme

2.1 Materials

The mud used in this study was taken from a storage yard in a coastal city in south China, with a natural water content of about 180%. The mud in the storage yard was originally generated from dredging construction by a cutter suction dredger. The relative density of soil particles (G_s) was determined as 2.66, and the liquid limit, plastic limit, and plasticity index were 61.26%, 26.34%, and 34.92, respectively, indicating a high-plasticity clay. In practice, various dredging techniques produce mud slurry with varying water content. The water content of dredged mud slurry is frequently 2~10 times the liquid limit. The initial water content of the mud slurry used in this study was artificially increased up to 300%, which is approximately 5 times the liquid limit and within the range of water content of dredged mud slurry obtained by typical dredging methods, like cutter suction dredging, bucket dredging and grab dredging.

GGBS used in this study is purchased from Wuxin New Building Materials Co., Ltd and the raw material to produce GGBS is blast furnace slag released from the pig iron smelting. The main chemical properties of raw materials, including mud slurry, cement, GGBS, hydrated lime, magnesium oxide (MgO) and carbide slag (CS), determined by X-ray fluorescence (XRF), are listed in Table 1. The main components of GGBS are CaO, SiO_2 and Al_2O_3, accounting for 41.42%, 32.60% and 14.04%, respectively, which are similar to the main components of cement. The main component of CS, i.e., calcium hydroxide, is the same as hydrated lime, with a relatively lower content.

2.2 Testing program

Three distinct treatment methods were included in the model test: VP method (mechanical only), BS method (chemical only) and VS combined method (mechanical-chemical combined). The testing program is shown in Table 2. Note that cement was used as the binder in the BS method case, abbreviated as BS-C. Cases VP and BS-C were designed as the control groups to compare the performance of the individual conventional method and the VS combined method. A vacuum pressure of -80 kPa was applied via PHD if vacuum preloading is involved.

Four types of binders, GGBS-lime, GGBS-MgO, GGBS-CS and cement, were used for the VS combined method test groups to investigate the effect of binder type on the performance of this method. For the solidification treatment of soft soils with high water content, the commonly used binder content ranges from 10% to 30% (Horpibulsuk, et al., 2005; Zhang et al., 2013) in practice, and in the present study, a relatively low binder amount of 10% was adopted. Additionally, different activator contents were used for the cases using GGBS-Lime, GGBS-MgO or GGBS-CS as binder, referring to the study by Yi et al. (2016), see Table 2 for the details. The mass ratio of cement or GGBS to dry soil is referred to as cement content or GGBS content, while the mass ratio of activator to GGBS is defined as activator content. The activator content is also included in the case No. for ease of understanding, for instance, in case VS-GL-10, VS is an acronym for **v**acuum-**s**olidification method, GL refers to **G**GBS-**L**ime as the binder, and 10 refers to the mass of hydrated lime that is **10**% of that of GGBS.

2.3 Testing procedure

The model test was conducted in a transparent plexiglass box with a wall thickness of 10 mm, and a length, width and height of 60 cm, 11 cm and 50 cm, respectively. To measure the volume change of the mud slurry during the vacuum consolidation process, three rulers are placed at equal spacings on the observation side of the model box. The control valve, water-air separator, and vacuum pump were connected to the model box in sequence through the drainage pipe, as shown in Fig. 3. The top of the model box was sealed with a flexible film before the vacuum preloading started. The model test used an integrated anti-clogging band drain produced by Jiangsu Xintai Geotechnical Technology Co., Ltd, with width and thickness of 100 mm and 4 mm, longitudinal water flow of 50 cm^3/s, dry state tensile strength of 6 MPa, and permeable rate of 0.33 s^{-1}, respectively. The band drain is placed at the bottom of the model tank in full, i.e., the model test simulates a one-dimensional vacuum consolidation.

Following are the specific test procedures:

First, the initial water content of the mud slurry was increased to 300% by adding tap water and mixing thoroughly.

Second, the binder was added to the mud slurry according to the test program, mixed thoroughly for ten minutes, and then poured into the model box and sealed the top with a flexible film, as shown in Fig. 3. For the cases utilizing alkali-activated GGBS as binder, the dry powder of activator and GGBS were well mixed before being added to the mud slurry.

Third, the vacuum preloading apparatus was connected as illustrated in Fig. 3, and then vacuum was applied in four sequent gradients of -10 kPa, -20 kPa, -40 kPa, and -80 kPa, with a

duration of half an hour for each level until the maximum vacuum pressure of -80 kPa was reached. Settlement of mud slurry and mass of discharged water were monitored during the 5-day vacuum preloading model test.

Forth, after the model test, a self-designed sampler was used to obtain the stabilized soil samples of 100 mm in height and 50 mm in diameter, as shown in Fig. 4. To reduce the disturbance to the soil during the sampling process, a sharp cutting edge was made at the end of the sampler, and Vaseline was applied evenly on the inner wall of the sampler.

Fifth, the obtained soil samples were sealed with plastic wrap and placed in a climatic chamber for curing. The temperature in the climatic chamber was kept at 20 ± 3°C, and the relative humidity was 95 ± 3%. The UC test was then performed on specimens after curing ages of 7, 14, 28, 60 and 90 days, and three parallel tests were conducted at each curing age, and the average value was taken as the test result. The UC test was performed with an axial strain rate of 1 mm/min, i.e., 1% of the initial height of the specimen per minute, in accordance with ASTM D 2166-00 (2002). For the control group, VP, the strength of treated soil decreased significantly with increasing distance from PHD band, resulting in the unavailability to take qualified samples for UC test. Therefore, three vane shear tests (H-60 hand-held vane shear tester, GEONOR, Inc., Norway) were conducted at 5 cm from the PHD band in VP. Twice the average shear strength was taken as the UCS of this case (Kang et al., 2015).

3 Results and discussions

3.1 Vacuum preloading dewatering

The vacuum dewatering efficiency for different cases was analyzed by comparing the mass of discharged water by vacuum m_{dw}, as shown in Fig. 5. Cases VP and VS-C are taken as references for comparison with cases using alkali-activated GGBS. The mass of discharged water for VP and VS-C after 4-day vacuum preloading is 9.1 kg and 10.7 kg, respectively. And Figs. 5(a), 4(b) and 4(c) indicate that the water mass of VS-GL-10, VS-GM-10 and VS-GC-10 is 14.9 kg, 15.1 kg and 16.1 kg, respectively, corresponding to 67 %, 67% and 78% higher than that of VP, and 36%, 36% and 45% higher than that of VS-C, respectively. Moreover, the mass of discharged water using VP method is the lowest during the 5-day vacuum preloading. The results well prove that the VS combined method is significantly better than the VP method in terms of vacuum dewatering efficiency, with a better performance using alkali-activated GGBS as binder than using cement.

The mass of discharged water in case VP kept increasing during the period of 5-day vacuum preloading with a lowering rate. however, it tends to be steady after 2.6 to 4.7 days of vacuum preloading for the cases using the VS combined method. In other words, the vacuum-solidification combined method has a restricted vacuum dewatering period, i.e., effective time of vacuum dewatering, t_e, beyond which there will be no visibly extra water discharged from mud slurry. Fig. 5 also demonstrates that the type of binder has an obvious effect on the effective time of vacuum dewatering. The vacuum-solidification combined method with cement as binder has a shorter t_e (2.5 days) than that with alkali-activated GGBS as binder.

277 Fig. 5 also demonstrates that t_e for cases using alkali-activated GGBS varies with the type
278 and content of activators, ranging from 2.6 ~ 4.7 days. The detailed effective time of vacuum
279 dewatering and the mass of discharged water after 5 days of vacuum preloading, m_{dw}, for cases
280 with different types and contents of activator are summarized in Table 3. The m_{dw} of the cases
281 using hydrated lime or MgO as activator is relatively close, ranging from 14.0 to 15.4 kg, and the
282 t_e reduces with increasing content of hydrated lime or MgO. Cases with CS as activator exhibit
283 the highest m_{dw} and t_e of around 16 kg and 4.7 days, respectively. The m_{dw} ratio and t_e ratio in
284 Table 3 are the ratios of m_{dw} and t_e for the cases with various activator types or amounts versus
285 VS-C. Compared with VS-C, it can be seen that, in general, a relatively large m_{dw} and a relatively
286 long t_e can be achieved at the same time when the amount of activators is around 10%.
287 After the completion of vacuum preloading, the water content of the upper, middle, and
288 lower of the soil layer in the model box was measured, and the water content reduction ratio was
289 calculated based on the average water content, as shown in Table 4. The water content results
290 correspond to the discharged water mass and settlement results. For the cases that used the VS
291 combined method, excluding case VS-C, the average water content was lower than that of the
292 vacuum preloading method (case VP). It should be noted that the vacuum consolidation of the
293 soil in the cases with binder has already ended, while based on the dewatering and settlement
294 results, the vacuum consolidation of case VP has not yet ended. Therefore, the water content of
295 case VP is not the final water content after the completion of vacuum consolidation.
296 The variation of vacuum dewatering rate with vacuum preloading time, as shown in Fig. 6,
297 provides a more intuitive indication of the effect of binder types on the vacuum dewatering

efficiency. The vacuum dewatering rate is defined as the ratio of the mass of discharged water at two consecutive recording time points to the corresponding time difference. For all cases, the vacuum dewatering rate decreased rapidly within one day after the start of vacuum preloading, because the hydraulic conductivity of mud slurry falls obviously due to the decreases in void ratio induced by vacuum consolidation. The sudden changes in the vacuum dewatering rate may be caused by (a) the non-homogeneity of the soil, which results in a non-smooth consolidation process, and the solidification reactions may exacerbate the non-smooth. The influence of the binder with hydrated lime as the activator on the consolidation process was greater than that with MgO. (b) Another possible reason could be the non-uniform interval of data collection and the error in collecting the data of mass of discharged water.

After one day of vacuum preloading, the vacuum dewatering rate for case VP dropped from 1.33 kg/hour to 0.06 kg/hour, corresponding to a reduction of 95%, and this reduction is noticeably greater than that for the cases using the VS combined method. It can be observed that the addition of binder slows the decreasing rate of the hydraulic conductivity of mud slurry during vacuum consolidation process. This is because, firstly, a significant amount of ions, such as Ca^{2+} and/or Mg^{2+}, etc., are produced during the hydration reaction of the binder, and the high-valent ions would replace the Na^{+} and K^{+} ions on the surface of the soil particles. As the surface potential of soil particles decreases, a thinner adsorption layer is formed so that soil particles aggregate into clusters, which is termed as flocculation (Prusinski and Bhattacharja, 1999; Jha et al., 2015). Secondly, the pozzolanic reaction produces stabilized compounds such as C-S-H and C-A-H, which bond the particles together to form a soil matrix with connecting pore channels (i.e.,

319 formation of soil skeleton) (Prusinski and Bhattacharja, 1999; Zhu et al., 2007), which enhances
320 to the permeability properties of the mud slurry (Quang and Chai, 2015).
321 However, the reduction of vacuum dewatering rate in cases using VS combined method
322 becomes faster after a period of vacuum preloading, with a lower vacuum dewatering rate than
323 case VS in two to five days of vacuum preloading, as shown in Fig. 6. This is because the
324 permeability improvement generated by flocculation and soil skeleton-building for cases with
325 binders is gradually diminishing. The reasons for the reduction of permeability improvement
326 effects are as follows: (*i*) the pozzolanic reaction procedure will continue to consume high-valent
327 ions, resulting in weakened flocculation; (*ii*) C-A-H/C-S-H and other solidification products
328 generated by the pozzolanic reaction make the structure of mud slurry denser, reducing the
329 permeability of mud slurry and leading to a decrease in vacuum dewatering rate. In addition, the
330 reduction rate of permeability improvement is closely related to the type of binder, with alkali-
331 activated GGBS exhibiting a slower reduction rate than cement. And a slower reduction rate
332 corresponds to a longer effective time of vacuum dewatering. This is attributed to the slower
333 reaction rate of alkali-activated GGBS solidification compared to that of cement (Yi et al., 2014).
334 Ca^{2+} has a higher cation exchange capacity than Mg^{2+} (Yi et al., 2016), therefore, the
335 flocculation effect produced by hydrated lime is higher than that of MgO, which is more helpful
336 for increasing the vacuum dewatering rate. This is the main reason for the slightly higher vacuum
337 dewatering rate in cases with hydrated lime as activator (Fig. 6a) than that of cases with MgO
338 (Fig. 6b) for a period of time after the start of vacuum preloading. The results also show that the
339 vacuum dewatering rate of cases with MgO as activator decreases faster than that of cases with

hydrated lime, as shown in the enlarged figures in Figs. 6(a) and 6(b). This is attributed to the higher efficiency of MgO in accelerating the hydration procedure of GGBS compared to hydrated lime (Yi et al., 2014). MgO is consumed faster to participate in the hydration procedure of GGBS than hydrated lime, resulting in a faster weakening of flocculation and a consequent reduction in the improvement of permeability induced by flocculation. Furthermore, the hydration products during the solidification procedure fill in the connecting pore channels, which also reduces the hydraulic conductivity of mud to some extent. Therefore, a faster rate of hydration reaction corresponds to a faster reduction rate of permeability. Compared with cases using hydrated lime as activator, cases with CS as activator has a lower vacuum dewatering rate, as shown in Fig. 6(c), with a slower reduction of vacuum dewatering rate. This is attributed to: (*i*) the main component of CS, calcium hydroxide, is the same as that in hydrated lime, but with a lower content, as shown in Table 1. The XRF results may overestimate the calcium hydroxide content of CS, because some amount of calcium carbonate may be present in CS (Cardoso et al., 2009). Both low calcium hydroxide content and the presence of less dissoluble calcium carbonate result in relatively weaker flocculation; (*ii*) the performance of CS as activator is weaker than that of hydrated lime, thereby slowing down the solidification process of CS-activated GGBS (Yi et al., 2014) and weakening the effects of flocculation and skeleton building.

The vacuum consolidation and binder are the main factors driving the variation in permeability of mud slurry for the VS combined method. It has been widely established that during vacuum consolidation, the void ratio decreases due to the drainage of pore water from the mud, resulting in a decrease in permeability. To investigate the influence of binder on the

permeability of mud slurry and to verify the above statement, the variable head permeability test using rigid wall permeameter was conducted using mud slurry with an initial water content of 93%. Song et al. (2000) and Yi et al. (2014) reported that the main hydration product of alkali-activated GGBS is C-S-H, similar to that of cement, regardless of the activator used. In addition, the permeability tests were mainly conducted to reveal the mechanism of the VS combined method. Therefore, cement was chosen as a representative of binders for the permeability test. To maintain the mud slurry in the device with the application of water head, the initial water content of mud slurry used in the permeability test is lower than that of model test. Fig. 7 shows the variation of the coefficient of permeability of mud slurry with different binder contents, A_w. The coefficient of permeability of mud slurry without binder decreases gradually with time due to the consolidation. The coefficient of permeability of the sample with A_w = 10% is 2.7 times higher than that of the sample without binder at day 0.5 and decreases rapidly over time. After 2.5 days, the coefficient is lower than that of the sample with A_w = 0%. This evidences that the addition of binder contributes to improving the permeability of mud slurry only within a period of time at the beginning of solidification reactions.

The settlement curves during vacuum preloading are shown in Fig. 8. Based on the settlement results, the variation of mud volume was obtained, and the dimensionless volume reduction results, i.e., the ratio of the reduced volume amount to the initial volume of mud, are illustrated in Fig. 9. The trend of mud volume reduction with vacuum preloading time corresponds to that of settlement of the mud layer. In the case of VP, the settlement of mud increased continuously throughout the entire 5-day vacuum preloading period, with a total settlement of

approximately 16.4 cm at the end, corresponding to a volume reduction of 41%. Even though the mass of discharged water of VS-C is more than that of VP (Fig. 5), the settlement (volume reduction) of case VS-C is less than that of VP. This is because the hydration products of the stabilization procedures of binder bind the soil particles and fill the pores between soil particles, resulting an increase in the strength of soil matrix to resist the settlement induced by soil consolidation (Ouhadi et al., 2014). However, in the cases using alkali-activated GGBS as binder, the settlement and volume reduction is much greater than that of VP and V-SC-10, which is consistent with the results of vacuum dewatering efficiency (Fig. 5) because the vacuum dewatering rate is faster and effective dewatering time is longer when alkali-activated GGBS is used as binder. The volume reduction in cases VS-GL-10 (Fig. 9a), VS-GM-10 (Fig. 9b) and VS-GC-10 (Fig. 9c) after 3-days vacuum preloading are 48%, 45% and 44%, respectively, which are 60%, 50% and 47% higher than that of VS-C, and 45%, 36% and 33% higher than that of VP. The greater settlement and volume reduction was observed when lime is used as activator, while the settlement and volume reduction is comparable when MgO and CS are used as activator. Although the addition of binder reduces the settlement caused by vacuum consolidation, the volume reduction of the VS combined method using alkali-activated GGBS is still larger than that of the VP method during the 5 days of vacuum preloading, which is mainly attributed to the substantial increase in vacuum dewatering efficiency by the alkali-activated GGBS. Therefore, the settlement and volume reduction are considerably influenced by the permeability improvement effect and reaction rate of binder, with a larger volume reduction for larger permeability improvement and slower hydration rate.

3.2 Unconfined compressive strength

Fig. 10 shows the unconfined compressive strength (UCS) at 7, 14, 28, 60 and 90 days for the stabilized soil of cases using VS combined method with alkali-activated GGBS as binder. Cases VP, BS-C and VS-C are taken as references for the comparison of strength improvement of VS combined method with alkali-activated GGBS as binder. It can be easily observed that the UCS of the soil samples treated by the VS combined method are much higher than their counterparts treated by the BS method and VP method. For instance, the 90-day UCS for cases VS-GL-10 (Fig. 10a), VS-GM-10 (Fig. 10b) and VS-GC-10 (Fig. 10c) are 859 kPa, 340 kPa and 310 kPa, respectively, which are 51, 20 and 18 times higher than that of BS stabilized soil using cement as binder, and 78, 31 and 28 times higher than that of case VP, respectively. It is evident that the performance of VS combined method in terms of strength development is significantly better than that of the VP and BS methods. It should be noted that, unlike cases with binder addition, the vacuum consolidation of case VP has not yet been completed. If the duration of vacuum preloading is extended, the soil strength of case VP will continue to increase. The UCS of the soil in case VP theoretically and empirically can reach 40~50 kPa after the completion of vacuum consolidation. The VP method and BS method are two commonly used techniques for strengthening soft soils, each with its own advantages. The VP method is relatively cost-effectively compared to other soil improvement techniques and has minimal environmental impact. On the other hand, the BS method can provide an immediate increase in soil strength and stiffness, making it a suitable option for areas where time constraints are critical. The VS method combines the advantages of both VP and BS methods. Compared to the VP method, the VS

combined method can increase soil strength more rapidly and compared to the BS method, it reduces the amount of binder used.

For the VS combined method, the 90-day UCS of the stabilized soil using alkali-activated GGBS is increased by 3.3 ~ 11.2 times compared to that with cement as binder. It can be concluded that in the VS combined method, alkali-activated GGBS outperforms cement in improving strength. This is attributed to (*i*) in regards to the binder itself, the solidification performance of alkali-activated GGBS is significantly better than that of cement, given the same initial conditions of the soil (e.g., water content and density) (Yi et al., 2014); (*ii*) the alkali-activated GGBS exhibited better performance in terms of vacuum dewatering (Table 3) and volume reduction (Fig. 9) compared to cement, resulting in a relatively lower water content and denser soil matrix after vacuum preloading, which further enhances the solidification capacities of alkali-activated GGBS.

The UCS of stabilized soil generally increases with curing time. In the cases of cement-stabilized soils (VS-C and BS-C), their strength reaches a peak at 28 days and stabilizes at 60 days. For alkali-activated GGBS stabilized soils, the strength development varies slightly depending on the activator/GGBS ratio. However, by 60 days of curing, the strength of the stabilized soils is close to its peak or stabilizes. Based on the specific initial water content and binder amount used in this study, a curing time of 60 days appears to be the ideal choice. In practical engineering, the optimal curing time needs to be determined based on the type and amount of binder, the initial water content of soil, the intended use of the treated soil, etc.

444 Furthermore, a systematic investigation is needed to better understand the influence of these
445 factors on the performance of the VS combined method.

446 The UCS of the stabilized soil increases nonlinearly with increasing lime content, as shown
447 in Fig. 10(a). The 90-day UCS of VS-GL-10 and VS-GL-20, are 657 kPa and 431 kPa,
448 respectively. It is well established that relatively low water content and a dense soil matrix
449 contribute to the strength development of stabilized soil. When the lime content is 10%, compared
450 to the case with 20% lime, the mass of discharged water (Table 3) and volume reduction (Fig. 9a)
451 is larger, corresponding to lower water content and a denser soil matrix after vacuum preloading.
452 And this is the reason for the larger UCS of VS-GL-10 than VS-GL-20. The UCS of soil stabilized
453 with GGBS-MgO (Fig. 10b) and GGBS-CS (Fig. 10c), especially at early curing ages, increased
454 significantly as the increases of activator content because a higher activator content results in a
455 faster reaction and higher volume of hydrates. Yi et al. (2014) reported that reactive MgO
456 activates GGBS at a higher rate than hydrated lime and achieves a higher strength of stabilized
457 soil. This conclusion, however, contradicts the findings of the present study. The strength of soil
458 stabilized with GGBS-MgO is slightly lower than that of soil stabilized with GGBS-lime. This is
459 attributed to the lower water content and denser matrix of mud with GGBS-lime after vacuum
460 dewatering (see Table 3, Figs. 8a and 8b), which is more favorable to the improvement of strength.
461 Compared to the strength of GGBS-lime and GGBS-MgO stabilized soil, GGBS-CS stabilized
462 soil has the lowest UCS at the same age. This is because MgO could activate GGBS more
463 efficiently than CS to achieve higher strength (Yi et al., 2015). And hydrated lime has a higher

464 calcium hydroxide content than that of CS, as indicated in Table 1, and thus has a higher activation
465 efficiency for hydration reaction of GGBS.
466 The pH of discharged water during the vacuum preloading was measured and presented in
467 Table 5. For hydrated lime, MgO and CS, pH values increase from 11.53, 9.45 and 9.17 to 12.16,
468 11.59 and 11.92, respectively when the activator content is increased from 10% to 20%. The
469 results indicate that, for each activator, the pH value increases with increasing activator content.
470 The pH of cases with GGBS-lime as binder is higher than that of cases using GGBS-MgO at the
471 same activator content, due to the difference between alkalinities of hydrated lime and MgO (Jin
472 and Al-Tabbaa, 2014). Although the main chemical composition of CS is similar to that of lime,
473 the pH of cases using GGBS-CS as binder is lower than that of cases using GGBS-lime because
474 lime has a larger calcium hydroxide content (Table 1). Song et al. (2000) summarized that higher
475 pH of solution leads to a higher activation reaction rate and degree of hydration of GGBS, and
476 Chrysochoou et al. (2010) reported that the UCS of stabilized soil is relatively small at a pH below
477 10.8. Combining the pH results of discharged water in Table 5 and the UCS results of stabilized
478 soil in Fig. 10, it can be observed that, in general, the increase of activator content increases the
479 pH of pore water and stabilized soil strength, especially for the early strength. Besides, a pH
480 adjustment is needed for the disposal of water because the pH of the pore water exceeds the
481 effluent limitation. In the initial stage of solidification reaction, the pH of the stabilized soil is
482 close to that of the pore water. However, as the solidification reactions process, the OH^- produced
483 by the binder is consumed to generate more solidification products. While the strength of

stabilized soil increases with curing age, the pH of the stabilized soil also decreases obviously (Cai et al., 2019; Feng et al., 2021).

3.3 Microstructure of stabilized soils

The 90-day crystalline phases, determined by X-ray diffraction (XRD) analysis, are illustrated in Fig. 11 for the stabilized soil using VS combined method and BS method with cement as binder. Calcite (C), illite (I), kaolinite (K) and quartz (Q) are detected as the principal minerals in all of the stabilized soil, representing the nature of the clay. C-S-H was detected in the cement-stabilized soil and also in the alkali-activated GGBS-stabilized soil regardless of the type of activator, which is consistent with the statements from previous studies (Song et al., 2000; Yi et al., 2014). Fig. 11(a) shows that the main hydration products of 90-day GGBS-lime stabilized soil include calcium aluminate hydrates (C-A-H), ettringite (E) and C-S-H, which are almost the same as those of cement stabilized soil. Calcium hydroxide is absent in the GGBS-lime stabilized soil at 90 days even with a lime/GGBS ratio as high as 40% due to the consumption of Ca^{2+} and OH^- during the activation of GGBS. C-S-H is the only detected hydration product in the GGBS-MgO stabilized soil, as shown in Fig. 11(b). Both of MgO and brucite ($Mg(OH)_2$) are not detected in 90-day GGBS-MgO stabilized soil because Mg^{2+} and OH^- are produced by MgO-water reaction directly without precipitation of brucite, and are consumed to activate GGBS (Yi et al., 2014). The hydration products of GGBS-CS stabilized soil (Fig. 11(c)), including C-A-H, C-S-H and ettringite, are similar to those of GGBS-lime stabilized soil because the main composition of carbide slag is also $Ca(OH)_2$ as indicated by the XRF results in Table 3. Similar to the GGBS-lime stabilized soil, $Ca(OH)_2$ is absent in the 90-day GGBS-CS stabilized soil. This is because

505 the consumption of Ca^{2+} and OH^- is not only involved in the activation of GGBS, but also in the
506 reactions of lime-soil. In other words, the role of hydrated lime is both an activator and a binder.
507 Typical SEM micrographs of stabilized soil in cases BS-C, VS-GL-10, VS-GM-10, VS-GC-
508 10 and VS-C at 90 days, as well as the treated soil in case VP, are shown in Fig. 12. The soil
509 sample treated by VP method, loose soil matrix without stabilization products, can be clearly seen
510 in Fig. 12(a). For the soil treated with the BS method, Fig. 12(b) displays a sparse surface
511 morphology with large pores among soil particles, despite the fact that the soil particles are
512 bonded with each other to some extent and some pores are filled by the hydration products of
513 cement (mainly C-S-H/C-A-H gel and needle-like ettringite), but not enough to develop a
514 relatively high strength because of the high porosity. The soil treated by the VS combined method
515 with GGBS-lime as binder (Fig. 12(c)) exhibits a dense surface morphology with soil particles
516 well bonded with each other and pores well filled by the hydration products of GGBS-lime, which
517 contributes to the development of high strength. A similar packing morphology of the stabilized
518 soil using GGBS-MgO as binder can be observed in Fig. 12(d). However, the needle-like
519 ettringite is absent in this case, which corresponds to findings by Yi et al. (2016), who reported
520 that the main hydration product of GGBS-MgO is C-S-H. Compared to the packing morphology
521 of stabilized soil for case VS-GL-10, a similar hydration product is found in the stabilized soil
522 with GGBS-CS as shown in Fig. 12(e), but the particles are relatively loosely packed. Importantly,
523 VS combined method produces a denser structure (refer to Figs. 11b and 11f) for the stabilized
524 soil compared to those using BS method, when cement is utilized as binder for both cases.

525 Fig. 13(a) presents the mercury intrusion curves for the soil samples at 90 days in cases BS-
526 C, VS-C, VS-GL-10, VS-GM-10 and VS-GC-10. The increase of the cumulative pore volume of
527 VS-C, VS-GL-10, VS-GM-10 and VS-GC-10 stabilized soil samples is mainly concentrated in
528 the range of radius ≤ 2000 μm, and the VS-C stabilized soil sample has the largest total intrusion
529 volume, because of the low vacuum dewatering efficiency and relatively limited solidification
530 effect of cement. The total porosities of the stabilized soil in case VS-GM-10 and case VS-GC-
531 10 are comparable, and slightly greater than that of VS-GL-10, which corresponds to the UCS
532 results shown in Fig. 10. It should be noted that the stabilized soil sample using BS method has a
533 significantly different mercury intrusion curve from the other cases. Despite the total intrusion
534 volume of BS-C stabilized soil is the smallest, its accumulated pore volume in relatively large-
535 size entrance pore radius ranging from 2000 μm to 4×10^4 μm is significantly greater than that of
536 VS-C, VS-GL-10, VS-GM-10 and VS-GC-10, which indicates that the volume of large-size pore
537 of BS-C stabilized soil is the largest, corresponding to the lowest UCS (Fig. 10).
538 Fig. 13(b) shows the differential pore size distribution of the stabilized soil. The amount of
539 relatively large-size pore ($10^3 \sim 3\times10^5$ μm) of the stabilized soil in case BS-C are significantly
540 greater than those in cases VS-C, VS-GL-10, VS-GM-10 and VS-GC-10 at the same age, which
541 is attributed to the absence of vacuum consolidation in BS-C. Compared with the VS-C, the VS-
542 GL-10, VS-GM-10 and VS-GC-10 stabilized soil samples have a small amount of pores with a
543 radius larger than 300 μm, but a larger amount of pores with a radius ranging from 10 ~ 200 μm.
544 This is mainly attributed to the higher improvement in vacuum dewatering and strength
545 development produced by alkali-activated GGBS. In particular, the VS-GL-10 stabilized soil has

546 the highest amount of small-size pores with a radius ranging from 10 ~ 60 μm, and the lowest
547 amount of large-size pores with a radius larger than 100 μm, which corresponds to the highest
548 UCS. In addition, in the cases of VS-GM-10 and VS-GC-10, stabilized soil samples have
549 relatively similar differential pore size distribution, however, the case VS-GM-10 contains more
550 pores with a radius of 10 ~ 80 μm and fewer pores with a radius of 80 ~ 300 μm, explaining the
551 higher UCS in VS-GM-10.

552 Fig. 14 illustrates the mercury intrusion and differential pore size distribution, respectively,
553 for the cases VS-GL-10, VS-GM-10 and VS-GC-10 at 28 and 90 days. Fig. 14(a) shows that the
554 porosity of stabilized soil in case VS-GL-10 decreases significantly from 28 to 90 days because
555 of the continuous hydration reactions produced by GGBS, corresponding to an obvious increase
556 in UCS. Although the total porosity of the VS-GM-10 and VS-GC-10 stabilized soil does not
557 change considerably from 28 to 90 days, the mercury intrusion curves shift downward between
558 radius ranging from 20 ~ 800 μm, indicating a decrease in cumulative volume of pores at the
559 corresponding radius. A decrease of large-size pores (100 ~ 500 μm) and an increase of small-
560 size pores (10 ~ 80 μm), as presented in Fig. 14(b), are observed for the stabilized soil from 28 to
561 90 days, which can be attributed to the production of ettringite or C-S-H-like compounds
562 produced by GGBS hydration reaction.

563 The main objective of this study is to investigate the feasibility and treatment effects of the
564 VS combined method with alkali-activated GGBS as binder and analyze its mechanism. However,
565 it should be noted that the model test has its limitations and there are many factors that affect the
566 treatment effect of this method, such as the thickness of slurry layer, initial water content, dosage

of binders, start time of vacuum dewatering, etc., which are not yet clear and will be the focus of the further research. One the other hand, despite the efficient and effective treatment of the VS combined method, the use of binders usually increases the pH of soil after treatment, which may have harmful effects on the environment, such as threatening the quality of groundwater or limiting the growth of vegetation, as well as the high carbon footprint of binder production (Latifi et al., 2017; Behnood, 2018; Jalal et al., 2020). Therefore, in the process of using the VS combined method, it is meaningful to use a low pH and low carbon footprint binder, such as MgO-GGBS, while meeting the engineering treatment requirements. Hence, the development of environmentally friendly binders for the VS combined method is also a subject for further research.

4 Conclusions

In this paper, the performance of the vacuum-solidification (VS) combined method using alkali-activated GGBS for treating mud slurry with high water content was investigated by model tests, and compared with the vacuum preloading (VP) method and binder solidification (BS) method. The following primary conclusions are drawn:

(1) VP method stands out for its cost-effectiveness and minimal environmental impact compared to other soil improvement approaches. On the other hand, the BS method provides rapid improvement of soil strength, making it particularly suitable for time-sensitive projects. Vacuum-solidification (VS) method combines the advantages of both VP and BS methods. During the limited duration of vacuum preloading testing (5 days), the VS combined method

demonstrates superior dewatering efficiency (not the final dewatering capacity upon completion of vacuum consolidation) compared to the VP method.

(2) The initial hydration products of the binder play a crucial role in enhancing the permeability of slurry, thereby facilitating vacuum dewatering, and densifying the soil structure. This initial densification sets the stage for subsequent solidification reactions within the compacted soil matrix, resulting in a significant improvement in soil strength.

(3) The treatment effect of the VS combined method is significantly influenced by the type of binder, with the best performance achieved by lime-activated GGBS. When GGBS-lime is used as binder, the volume reduction is more than 40% greater than that when cement is used, and the UCS of treated soil is increased by more than 2.8 times. Therefore, the adoption of alkali-activated GGBS as binder instead of cement results in better treatment performance and is more in line with the requirements of sustainable development. The industrial by-product CS also can be used to replace hydrated lime as activator, but due to its low calcium hydroxide content, it is necessary to appropriately increase the activator content to achieve the expected improvement.

(4) The stabilized soil samples using GGBS-lime, GGBS-CS or cement have similar hydration products, including C-S-H, C-A-H and ettringite. The microstructure of soil treated by VS combined method is denser than that of soil treated with the VP and BS methods. Compared to the soil stabilized using cement, soil treated by VS combined method with alkali-activated GGBS has more small-size pores, fewer large-size pores and lower total porosity, which contributed to a significantly higher UCS.

Declaration of competing interest

The authors declare that they have no known competing financial interests or personal relationships that could have appeared to influence the work reported in this paper.

Data availability

Data will be made available on request.

Acknowledgments

This research was supported by the Research Grants Council of Hong Kong Special Administrative Region Government of China (Grant No.: 15209119, 15210322 and R5037-18). The authors also acknowledge the financial supports from grants (CD7A and CD82) from Research Institute for Land and Space of Hong Kong Polytechnic University and financial support from grant (BBEJ) from Research Centre for Resources Engineering towards Carbon Neutrality, and a grant (BD8U) from Hong Kong Polytechnic University.

References

Anand, S., Vrat, P., and Dahiya, R. P. (2006). Application of a system dynamics approach for assessment and mitigation of CO2 emissions from the cement industry. Journal of environmental management, 79(4), 383-398.

631 ASTM D 2166-00. (2002). Standard test method for unconfined compressive strength of cohesive
632 soil. In: Annual book of ASTM standards. American Society for Testing and Materials, West
633 Conshohocken, pp 1-6.
634 Behnood, A. (2018). Soil and clay stabilization with calcium-and non-calcium-based additives: A
635 state-of-the-art review of challenges, approaches and techniques. Transportation Geotechnics,
636 17, 14-32.
637 Cai, G., Liu, S., Du, G., and Wang, L. (2019). Effect of MgO activity index on physicochemical,
638 electrical and mechanical properties of carbonated MgO-admixed silt. KSCE Journal of Civil
639 Engineering, 23(9), 3807-3817.
640 Cai, Y., Qiao, H., Wang, J., Geng, X., Wang, P., and Cai, Y. (2017). Experimental tests on effect
641 of deformed prefabricated vertical drains in dredged soil on consolidation via vacuum
642 preloading. Engineering Geology, 222, 10-19.
643 Cardoso, F. A., Fernandes, H. C., Pileggi, R. G., Cincotto, M. A., and John, V. M. (2009). Carbide
644 lime and industrial hydrated lime characterization. Powder Technology, 195(2), 143-149.
645 Chai, J. C., Carter, J. P., and Hayashi, S. (2006). Vacuum consolidation and its combination with
646 embankment loading. Canadian Geotechnical Journal, 43(10), 985-996.
647 Chai, J. C., Hino, T., and Shen, S. L. (2017). Characteristics of clay deposits in Saga Plain, Japan.
648 Proceedings of the Institution of Civil Engineers-Geotechnical Engineering, 170(6), 548-558.
649 Chen, C., Habert, G., Bouzidi, Y., and Jullien, A. (2010). Environmental impact of cement
650 production: detail of the different processes and cement plant variability evaluation. Journal of
651 Cleaner Production, 18(5), 478-485.
652 Chen, L., Gao, Y., Elsayed, A., and Yang, X. (2019). Soil consolidation and vacuum pressure
653 distribution under prefabricated vertical drains. Geotechnical and Geological Engineering,
654 37(4), 3037-3048.
655 Chen, M., Ding, S., Gao, S., Fu, Z., Tang, W., Wu, Y., Gong, M., Wang, D. and Wang, Y. (2019).
656 Efficacy of dredging engineering as a means to remove heavy metals from lake sediments.
657 Science of the Total Environment, 665, 181-190.

Chiba, T., Shinsha, H. H., and Tani, Y. (1992). Development of a vacuum-consolidation method employing horizontal drains (No. AD-P-006467/5/XAB). Japan Dredging and Reclamation Engineering Association, Tokyo (Japan).

Chrysochoou, M., Grubb, D. G., Drengler, K. L., and Malasavage, N. E. (2010). Stabilized dredged material. III: Mineralogical perspective. Journal of Geotechnical and Geoenvironmental Engineering, 136(8), 1037-1050.

Chu, J., Yan, S., and Lam, K. P. (2012). Methods for improvement of clay slurry or sewage sludge. Proceedings of the Institution of Civil Engineers-Ground Improvement, 165(4), 187-199.

Correia, A. G., Winter, M. G., and Puppala, A. J. (2016). A review of sustainable approaches in transport infrastructure geotechnics. Transportation Geotechnics, 7, 21-28.

de Lillis, A., Fasano, G., Flora, A., and Miliziano, S. (2022). A novel application of vacuum preloading: conception, analysis and performance evaluation. Proceedings of the Institution of Civil Engineers-Ground Improvement, 1-16.

Deng, Y., Liu, L., Cui, Y. J., Feng, Q., Chen, X., and He, N. (2019). Colloid effect on clogging mechanism of hydraulic reclamation mud improved by vacuum preloading. Canadian Geotechnical Journal, 56(5), 611-620.

Feng, S. J., Du, F. L., Chen, H. X., and Mao, J. Z. (2017). Centrifuge modeling of preloading consolidation and dynamic compaction in treating dredged soil. Engineering Geology, 226, 161-171.

Feng, Y. S., Du, Y. J., Zhou, A., Zhang, M., Li, J. S., Zhou, S. J., and Xia, W. Y. (2021). Geoenvironmental properties of industrially contaminated site soil solidified/stabilized with a sustainable by-product-based binder. Science of the Total Environment, 765, 142778.

Gonzalez, J., Sargent, P., and Ennis, C. (2021). Sewage treatment sludge biochar activated blast furnace slag as a low carbon binder for soft soil stabilisation. Journal of Cleaner Production, 311, 127553.

Haha, M. B., Lothenbach, B., Le Saout, G. L., and Winnefeld, F. (2011). Influence of slag chemistry on the hydration of alkali-activated blast-furnace slag—Part I: Effect of MgO. Cement and Concrete Research, 41(9), 955-963.

686 Ho, T. O., Chen, W. B., Yin, J. H., Wu, P. C., and Tsang, D. C. (2021). Stress-strain behaviour of
687 cement-stabilized Hong Kong marine deposits. Construction and Building Materials, 274,
688 122103.
689 Ho, T. O., Tsang, D. C., Chen, W. B., and Yin, J. H. (2020). Evaluating the environmental impact
690 of contaminated sediment column stabilized by deep cement mixing. Chemosphere, 261,
691 127755.
692 Horpibulsuk, S., Miura, N., and Nagaraj, T. S. (2005). Clay–water／cement ratio identity for
693 cement admixed soft clays. Journal of geotechnical and geoenvironmental engineering, 131(2),
694 187-192.
695 Huang, Y., Zhu, W., Qian, X., Zhang, N., and Zhou, X. (2011). Change of mechanical behavior
696 between stabilized and remolded stabilized dredged materials. Engineering Geology, 119(3-4),
697 112-119.
698 Jalal, F. E., Xu, Y., Jamhiri, B., and Memon, S. A. (2020). On the recent trends in expansive soil
699 stabilization using calcium-based stabilizer materials (CSMs): a comprehensive review.
700 Advances in Materials Science and Engineering, 2020, 1-23.
701 Jha, A. K., and Sivapullaiah, P. V. (2015). Mechanism of improvement in the strength and volume
702 change behavior of lime stabilized soil. Engineering Geology, 198, 53-64.
703 Jin, F., and Al-Tabbaa, A. (2014). Characterisation of different commercial reactive magnesia.
704 Advances in cement research, 26(2), 101-113.
705 Kang, G., Tsuchida, T., and Athapaththu, A. M. R. G. (2015). Strength mobilization of cement-
706 treated dredged clay during the early stages of curing. Soils and Foundations, 55(2), 375-392.
707 Latifi, N., Horpibulsuk, S., Meehan, C. L., Abd Majid, M. Z., Tahir, M. M., and Mohamad, E. T.
708 (2017). Improvement of problematic soils with biopolymer - an environmentally friendly soil
709 stabilizer. Journal of Materials in Civil Engineering, 29(2), 04016204.
710 Lei, H., Wang, L., Jia, R., Jiang, M., Zhang, W., and Li, C. (2020). Effects of chemical conditions
711 on the engineering properties and microscopic characteristics of Tianjin dredged fill.
712 Engineering Geology, 269, 105548.

713 Lei, H., Xu, Y., Li, X., Jiang, M., and Liu, L. (2019). Effect of polyacrylamide on improvement
714 of dredger fill with vacuum preloading method. Journal of Materials in Civil Engineering, 31(9),
715 04019193.
716 Li, M., Chen, Q., Wen, K., Nimbalkar, S., and Dai, R. (2021). Improved vacuum preloading
717 method combined with sand sandwich structure for consolidation of dredged clay-slurry fill
718 and original marine soft clay. International Journal of Geomechanics, 21(10), 04021182.
719 Miura, N., Horpibulsuk, S., and Nagaraj, T. S. (2001). Engineering behavior of cement stabilized
720 clay at high water content. Soils and foundations, 41(5), 33-45.
721 Mymrin, V., Scremim, C. B., Stella, J. C., Pan, R. C., Avanci, M. A., Bosco, J. C., and Rolim, P.
722 (2021). Environmentally clean materials from contaminated marine dredged sludge, wood
723 ashes and lime production wastes. Journal of Cleaner Production, 307, 127074.
724 Ngo, D. H., Horpibulsuk, S., Suddeepong, A., Hoy, M., Chinkulkijniwat, A., Arulrajah, A., and
725 Chaiwan, A. (2020). Compressibility of ultra-soft soil in the Mae Moh Mine, Thailand.
726 Engineering Geology, 271, 105594.
727 Ouhadi, V. R., Yong, R. N., Amiri, M., and Ouhadi, M. H. (2014). Pozzolanic consolidation of
728 stabilized soft clays. Applied Clay Science, 95, 111-118.
729 Pacheco-Torgal, F., Castro-Gomes, J., and Jalali, S. (2008). Alkali-activated binders: A review:
730 Part 1. Historical background, terminology, reaction mechanisms and hydration products.
731 Construction and building Materials, 22(7), 1305-1314.
732 Proaño, L., Sarmiento, A. T., Figueredo, M., and Cobo, M. (2020). Techno-economic evaluation
733 of indirect carbonation for CO_2 emissions capture in cement industry: A system dynamics
734 approach. Journal of Cleaner Production, 263, 121457.
735 Prusinski, J. R., and Bhattacharja, S. (1999). Effectiveness of Portland cement and lime in
736 stabilizing clay soils. Transportation Research Record, 1652(1), 215-227.
737 Quang, N. D., and Chai, J. C. (2015). Permeability of lime-and cement-treated clayey
738 soils. Canadian Geotechnical Journal, 52(9), 1221-1227.
739 Rakshith, S., and Singh, D. N. (2017). Utilization of dredged sediments: contemporary issues.
740 Journal of Waterway, Port, Coastal, and Ocean Engineering, 143(3), 04016025.

741 Sato, T., and Kato, H. (2002). Application of the pneumatic flow mixing method to land
742 development for Central Japan International Airport. In Proceedings of the 2002 Interntional
743 Symposium on Underwater Technology (Cat. No. 02EX556) (pp. 93-98). IEEE.
744 Shinsha, H. and Kumagai, T. (2014). Bulk compression of dredged soils by vacuum consolidation
745 method using horizontal drains. Geotechnical Engineering Journal of the SEAGS & AGSSEA,
746 45(3), 78-85.
747 Siham, K., Fabrice, B., Edine, A. N., and Patrick, D. (2008). Marine dredged sediments as new
748 materials resource for road construction. Waste Management, 28(5), 919-928.
749 Snellings, R., Cizer, Ö., Horckmans, L., Durdziński, P. T., Dierckx, P., Nielsen, P., Van Balen
750 Koenradd, R. and Vandewalle, L. (2016). Properties and pozzolanic reactivity of flash calcined
751 dredging sediments. Applied Clay Science, 129, 35-39.
752 Song, D.B., Pu, H. F., Yin, Z. Y., Min, M., Qiu, J. W. (2023). Plane-strain model for large strain
753 consolidation induced by vacuum-assisted prefabricated horizontal drains. International
754 Journal for Numerical and Analytical Methods in Geomechanics, 00, 1-25.
755 Song, S., Sohn, D., Jennings, H. M., and Mason, T. O. (2000). Hydration of alkali-activated
756 ground granulated blast furnace slag. Journal of Materials Science, 35(1), 249-257.
757 Staniszewska, M., and Boniecka, H. (2017). Managing dredged material in the coastal zone of
758 the Baltic Sea. Environmental Monitoring and Assessment, 189(2), 1-17.
759 Sun, L., Gao, X., Zhuang, D., Guo, W., Hou, J., and Liu, X. (2018). Pilot tests on vacuum
760 preloading method combined with short and long PVDs. Geotextiles and Geomembranes,
761 46(2), 243-250.
762 Sun, Z., Chen, W. B., Zhao, R. D., Jin, Y. F., and Yin, J. H. (2023). Solidification/stabilization
763 treatment of Hong Kong marine deposits slurry at high water content by ISSA and GGBS.
764 Construction and Building Materials, 372, 130817.
765 Svensson, N., Norén, A., Modin, O., Fedje, K. K., Rauch, S., Strömvall, A. M., and Andersson-
766 Sköld, Y. (2022). Integrated cost and environmental impact assessment of management options
767 for dredged sediment. Waste Management, 138, 30-40.

768 Tang, C. S., Cheng, Q., Wang, P., Wang, H. S., Wang, Y., and Inyang, H. I. (2020). Hydro-
769 mechanical behavior of fiber reinforced dredged sludge. Engineering Geology, 276, 105779.
770 Umehara, Y., and Zen, K. (1982). Consolidation characteristics of dredged marine bottom
771 sediments with high water content. Soils and Foundations, 22(2), 40-54.
772 Wang, D., Abriak, N. E., and Zentar, R. (2017). Dredged marine sediments used as novel supply
773 of filling materials for road construction. Marine Georesources & Geotechnology, 35(4), 472-
774 480.
775 Wang, J., Huang, G., Fu, H., Cai, Y., Hu, X., Lou, X., ... and Zou, J. (2019). Vacuum preloading
776 combined with multiple-flocculant treatment for dredged fill improvement. Engineering
777 Geology, 259, 105194.
778 Wang, J., Ni, J., Cai, Y., Fu, H., and Wang, P. (2017). Combination of vacuum preloading and
779 lime treatment for improvement of dredged fill. Engineering Geology, 227, 149-158.
780 Wang, L., Chen, L., Tsang, D. C., Li, J. S., Baek, K., Hou, D., Ding, S. and Poon, C. S. (2018).
781 Recycling dredged sediment into fill materials, partition blocks, and paving blocks: Technical
782 and economic assessment. Journal of Cleaner Production, 199, 69-76.
783 Wu, P. C., Yin, J. H., Feng, W. Q., and Chen, W. B. (2019). Experimental study on geosynthetic-
784 reinforced sand fill over marine clay with or without deep cement mixed soil columns under
785 different loadings. Underground space, 4(4), 340-347.
786 Wu, T., Ng, S. T., and Chen, J. (2022). Deciphering the CO2 emissions and emission intensity of
787 cement sector in China through decomposition analysis. Journal of Cleaner Production, 352,
788 131627.
789 Xu, G., Gao, Y., Yin, J., Yang, R., and Ni, J. (2015). Compression behavior of dredged slurries at
790 high water contents. Marine Georesources & Geotechnology, 33(2), 99-108.
791 Yan, W. M., and Ma, Y. (2010). Geotechnical characterization of Macau marine deposits.
792 Engineering Geology, 113(1-4), 62-69.
793 Yi, Y., Liska, M., and Al-Tabbaa, A. (2014). Properties of two model soils stabilized with different
794 blends and contents of GGBS, MgO, lime, and PC. Journal of Materials in Civil Engineering,
795 26(2), 267-274.

796 Yi, Y., Liska, M., Jin, F., and Al-Tabbaa, A. (2016). Mechanism of reactive magnesia–ground
797 granulated blastfurnace slag (GGBS) soil stabilization. Canadian Geotechnical Journal, 53(5),
798 773-782.
799 Yi, Y., Zheng, X., Liu, S., and Al-Tabbaa, A. (2015). Comparison of reactive magnesia-and
800 carbide slag-activated ground granulated blastfurnace slag and Portland cement for
801 stabilisation of a natural soil. Applied Clay Science, 111, 21-26.
802 Yoobanpot, N., Jamsawang, P., Poorahong, H., Jongpradist, P., and Likitlersuang, S. (2020).
803 Multiscale laboratory investigation of the mechanical and microstructural properties of dredged
804 sediments stabilized with cement and fly ash. Engineering Geology, 267, 105491.
805 Zhang, R. J., Santoso, A. M., Tan, T. S., and Phoon, K. K. (2013). Strength of high water-content
806 marine clay stabilized by low amount of cement. Journal of Geotechnical and
807 Geoenvironmental Engineering, 139(12), 2170-2181.
808 Zhang, R. J., Zheng, Y. L., Dong, C. Q., and Zheng, J. J. (2022). Strength behavior of dredged
809 mud slurry treated jointly by cement, flocculant and vacuum preloading. Acta Geotechnica,
810 17(6), 2581-2596.
811 Zhang, R. J., Zheng, Y. L., Zheng, J. J., Dong, C. Q., and Lu, Z. (2020). Flocculation–
812 solidification combined method for treatment of hydraulically dredged mud at extra high water
813 content. Acta Geotechnica, 15(6), 1685-1698.
814 Zhu, W., Zhang, C. L., and Chiu, A. C. (2007). Soil–water transfer mechanism for solidified
815 dredged materials. Journal of Geotechnical and Geoenvironmental Engineering, 133(5), 588-
816 598.

List of Figures

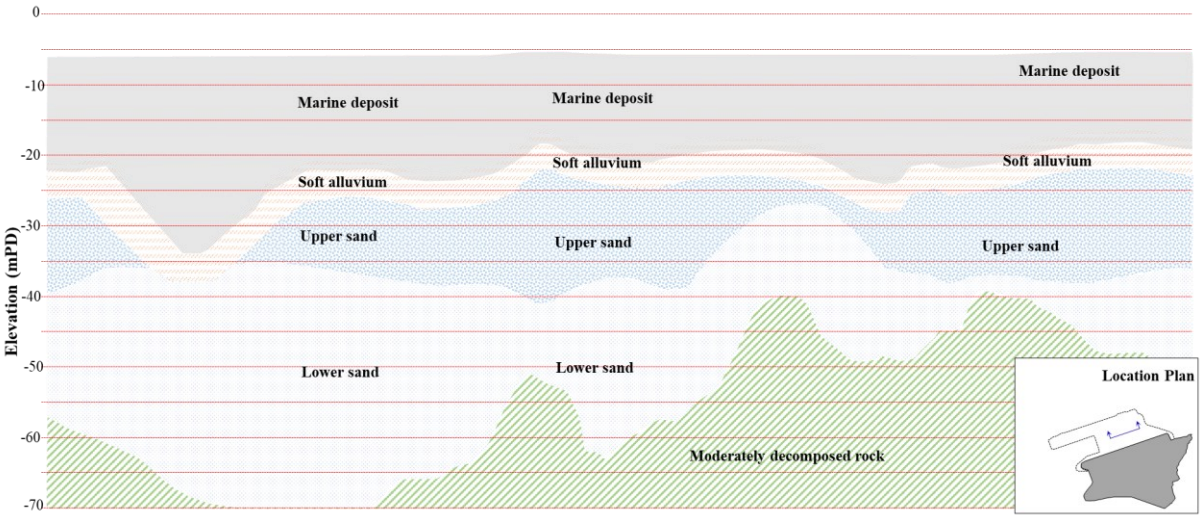

Fig. 1 Geological cross-section of Hong Kong International Airport site

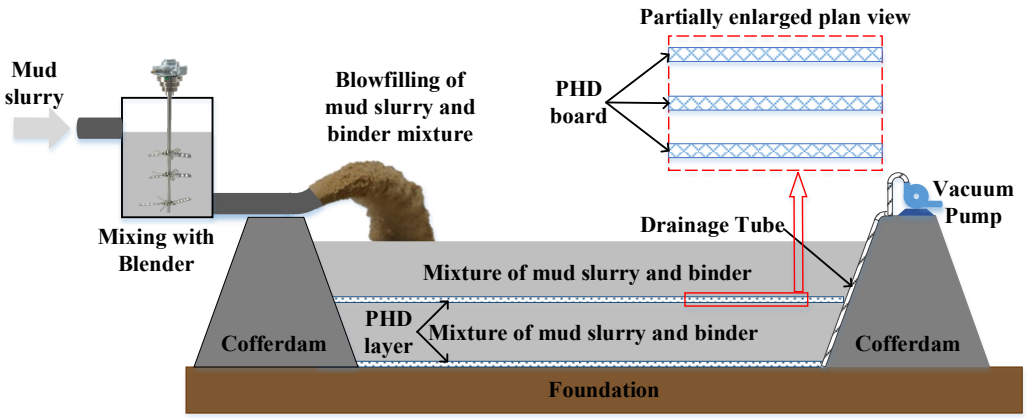

Fig. 2 Schematic diagram of the vacuum-solidification combined method based on PHD

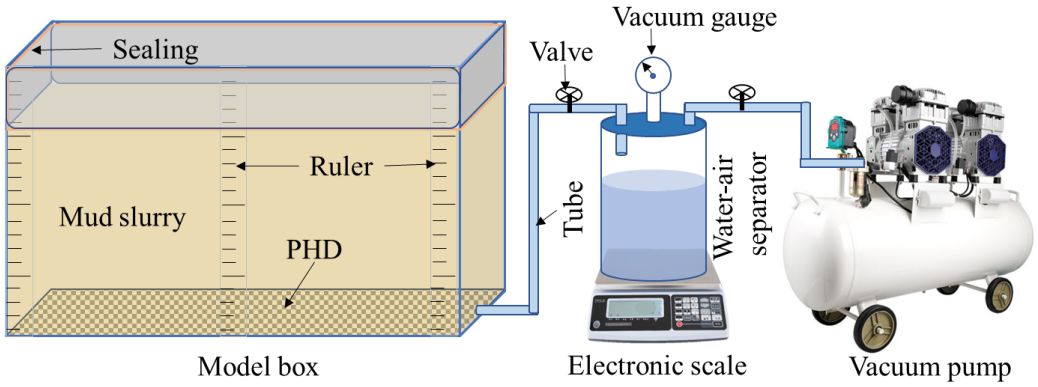

Fig. 3 Schematic diagram of the model test

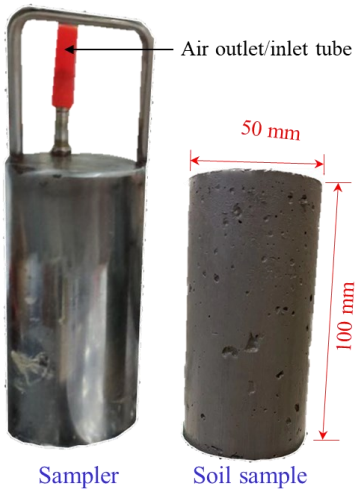

Fig. 4 Photographs of the sampler and stabilized soil sample after vacuum preloading

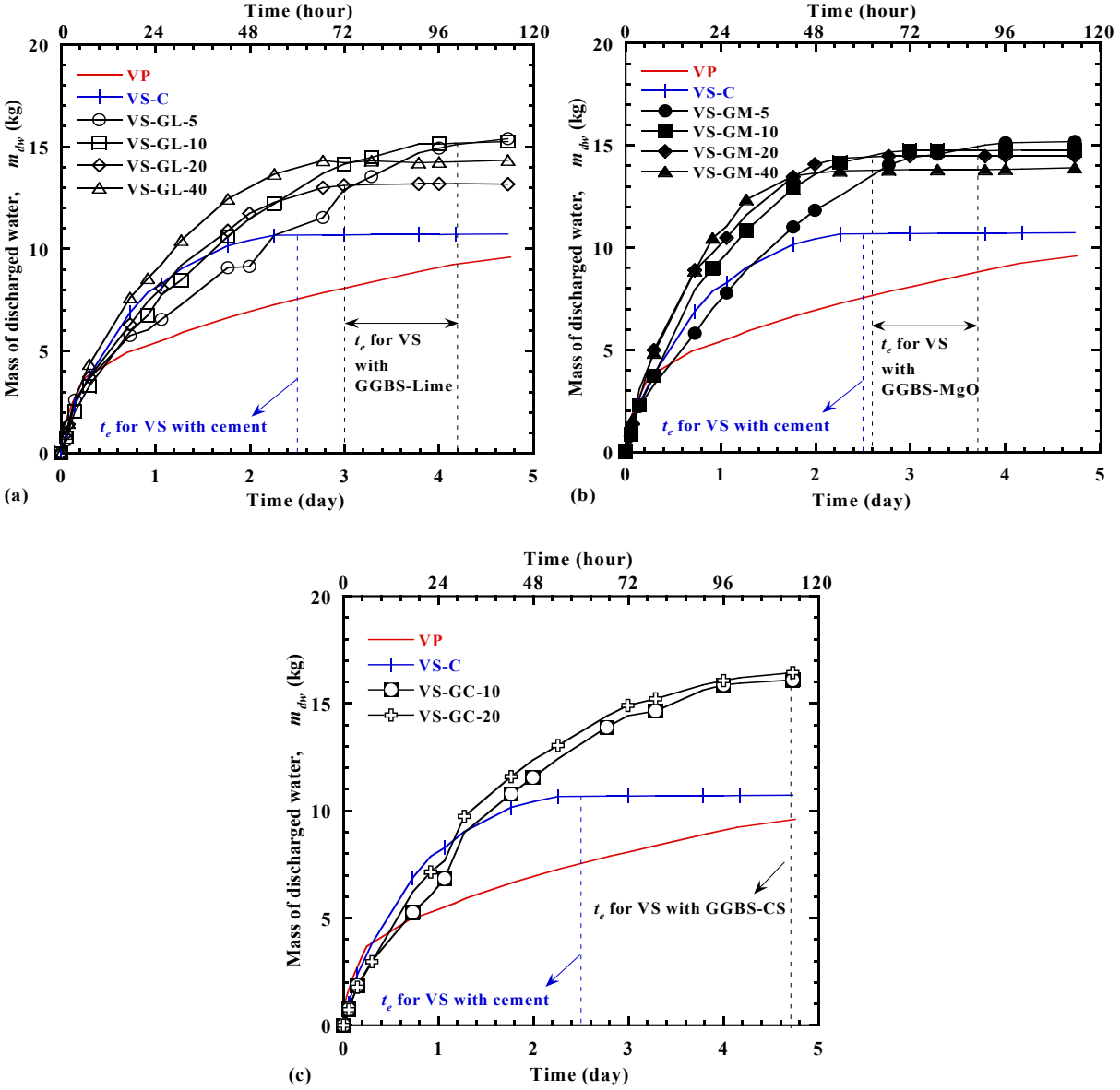

Fig. 5 Comparison of mass of discharged water between VP, VS-C and cases with (a) GGBS-Lime, (b) GGBS-MgO, and (c) GGBS-CS as binder

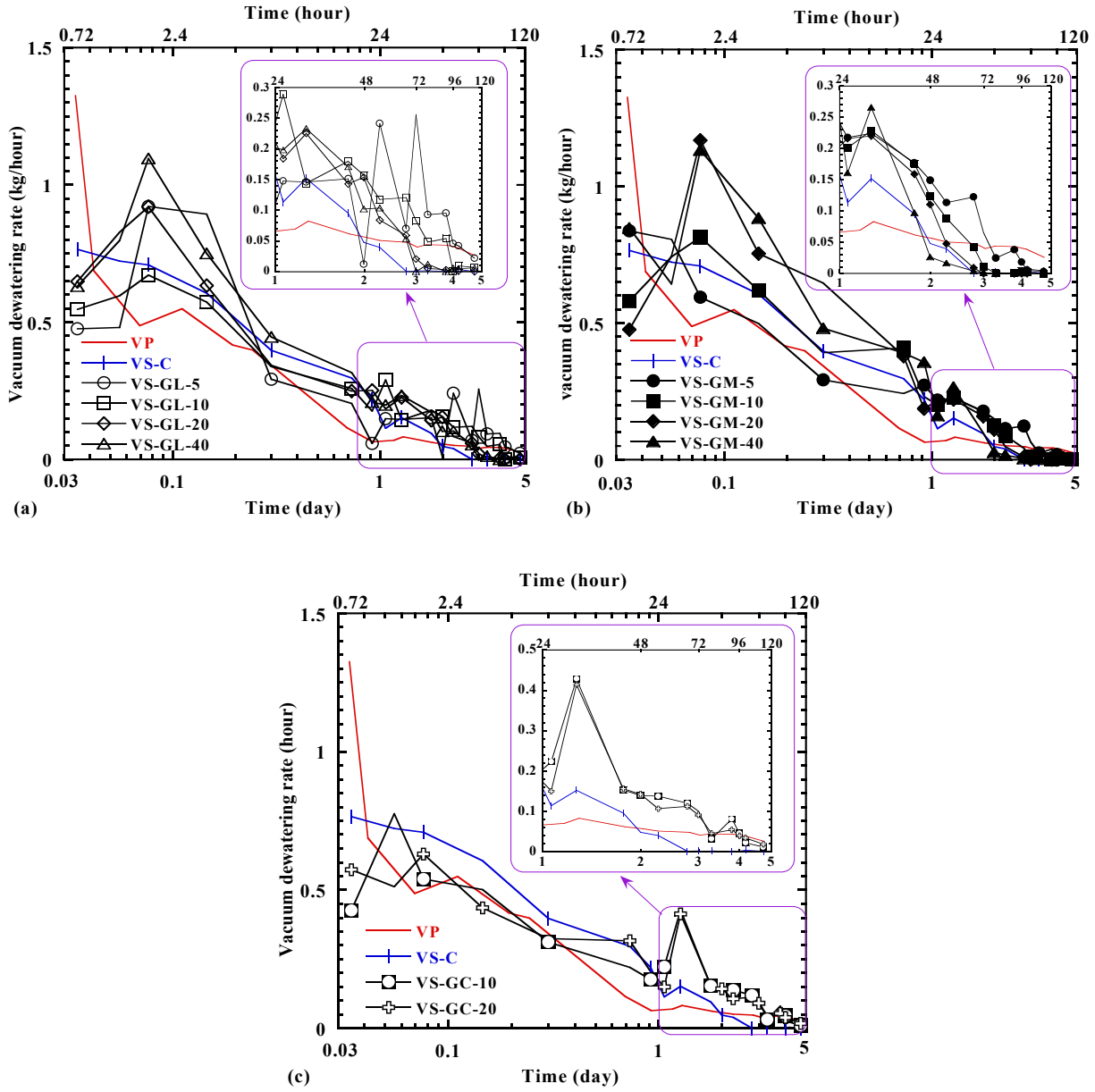

Fig. 6 Comparison of vacuum dewatering rate between VP, VS-C and cases with (a) GGBS-Lime, (b) GGBS-MgO, and (c) GGBS-CS as binder

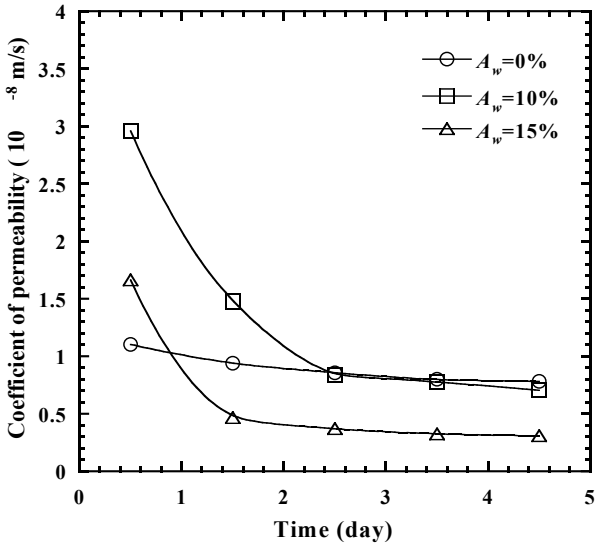

Fig. 7 Variation of the permeability coefficient with time for mud samples with different binder contents

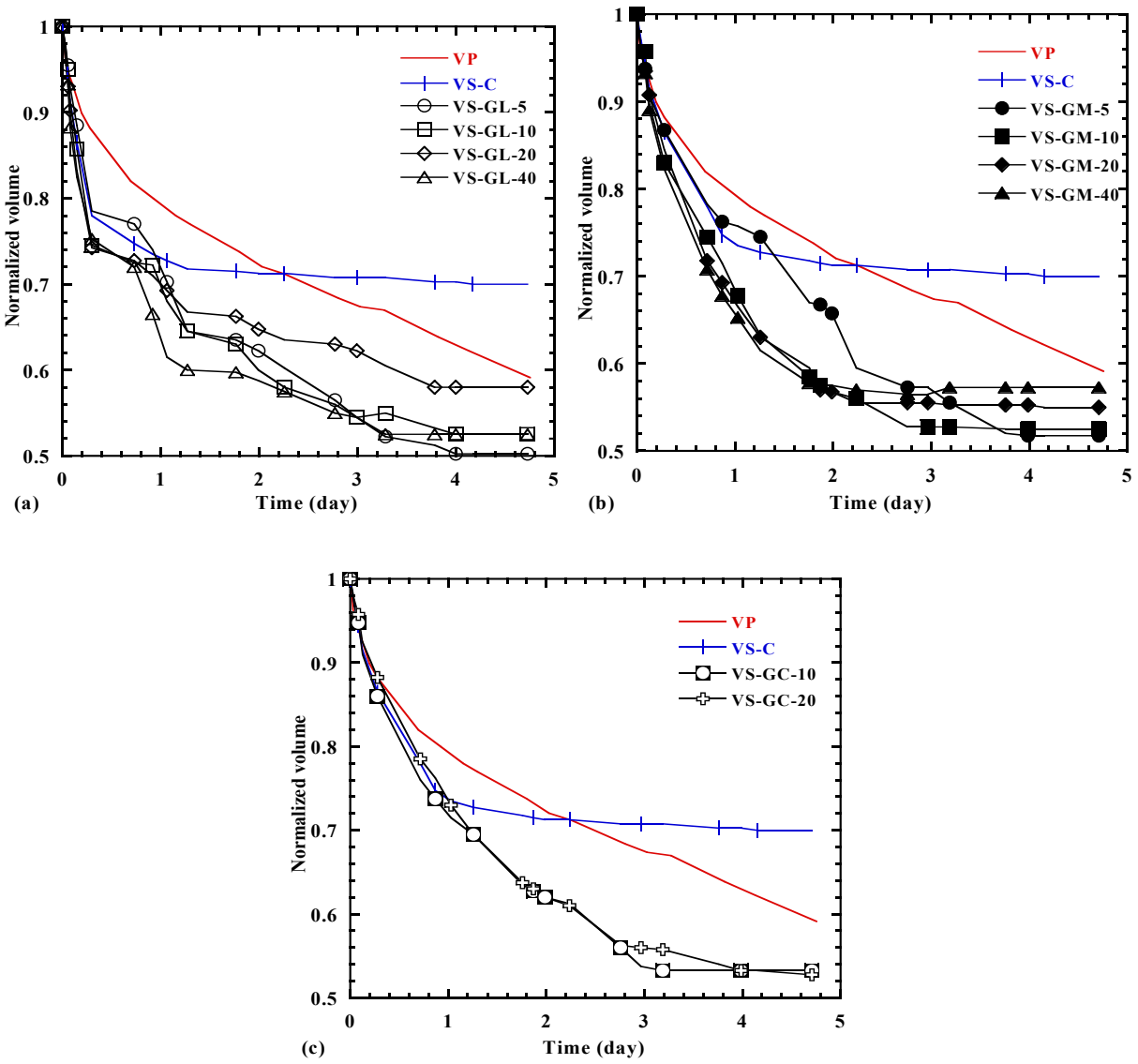

Fig. 8 Comparison of volume reduction between VP, VS-C and cases with (a) GGBS-Lime, (b) GGBS-MgO, and (c) GGBS-CS as binder

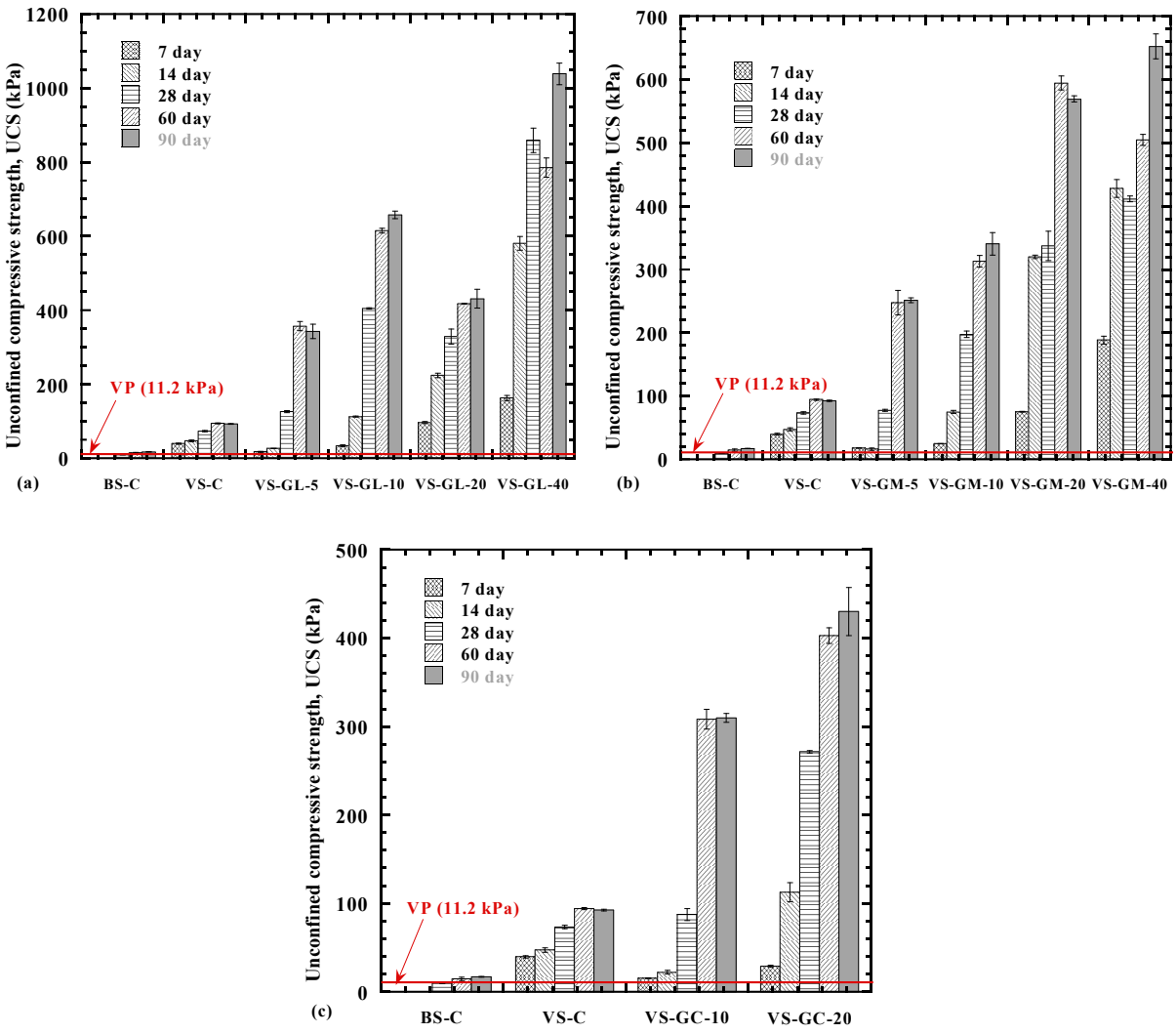

Fig. 9 Comparison of UCS between soil samples of VP, BS-C, VS-C and cases with (a) GGBS-Lime, (b) GGBS-MgO, and (c) GGBS as binder

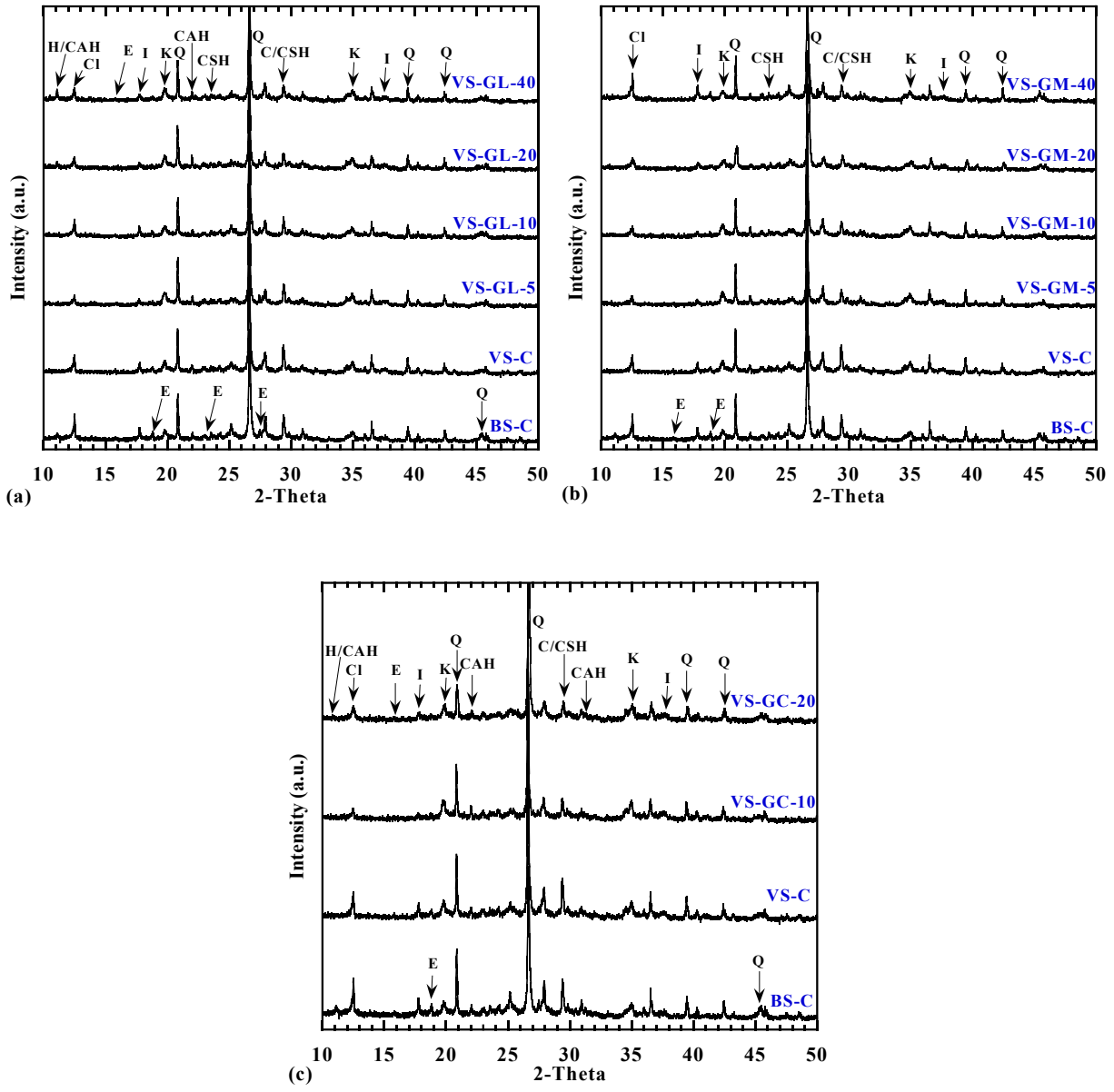

Fig. 10 XRD diffractograms of the stabilized soils at 90 days for BS-C, VS-C and cases with (a) GGBS-Lime, (b) GGBS-MgO, and (c) GGBS as binder. (The abbreviations stand for CI-clinochlore, C-calcite, CAH-calcium culminate hydrates, CSH-calcium silicate hydrates, E-ettringite, H-hydrocalumite, I-illite, K-kaolinite, Q-quartz)

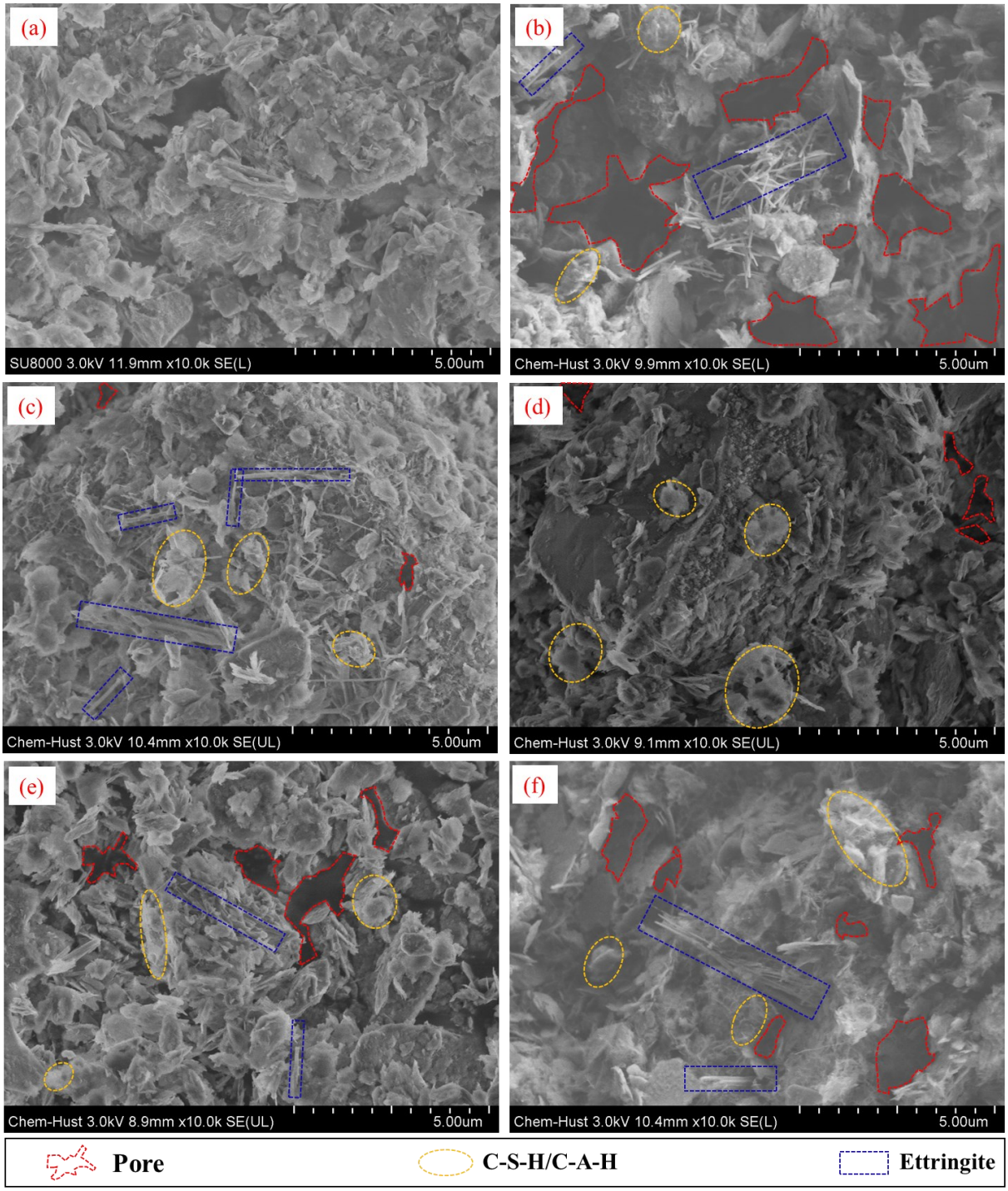

Fig. 11 SEM Micrographs of the treated soil at 90 d for: (a) VP, (b) BS-C, (c) VS-GL-10, (d) VS-GM-10, (e) VS-GC-10, and (f) VS-C

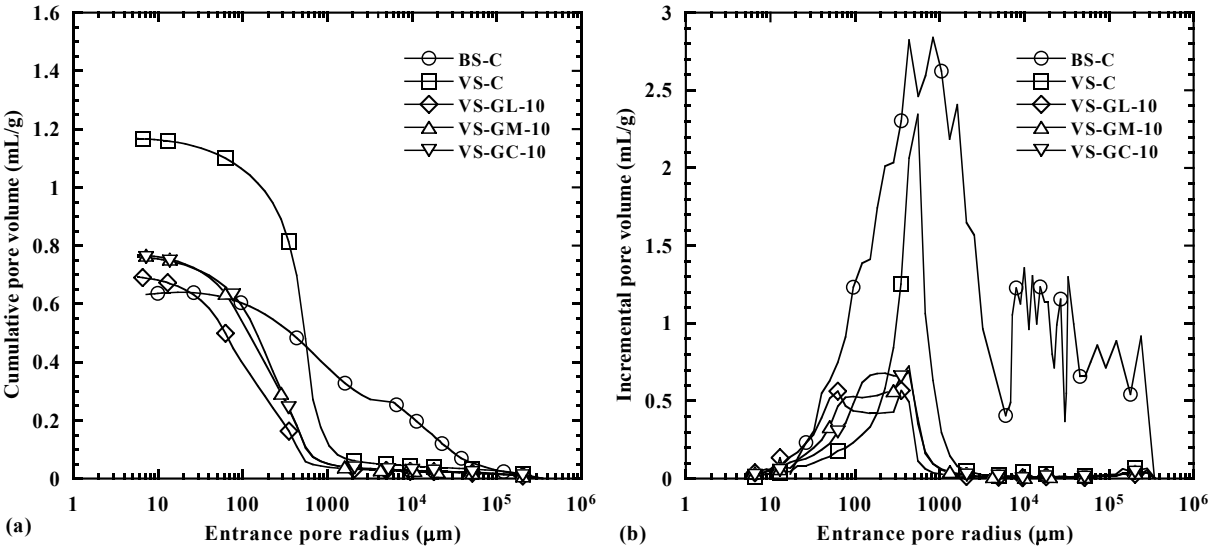

Fig. 12 MIP results for selected stabilized soil at days (a) mercury intrusion curves and (b) differential pore size distribution

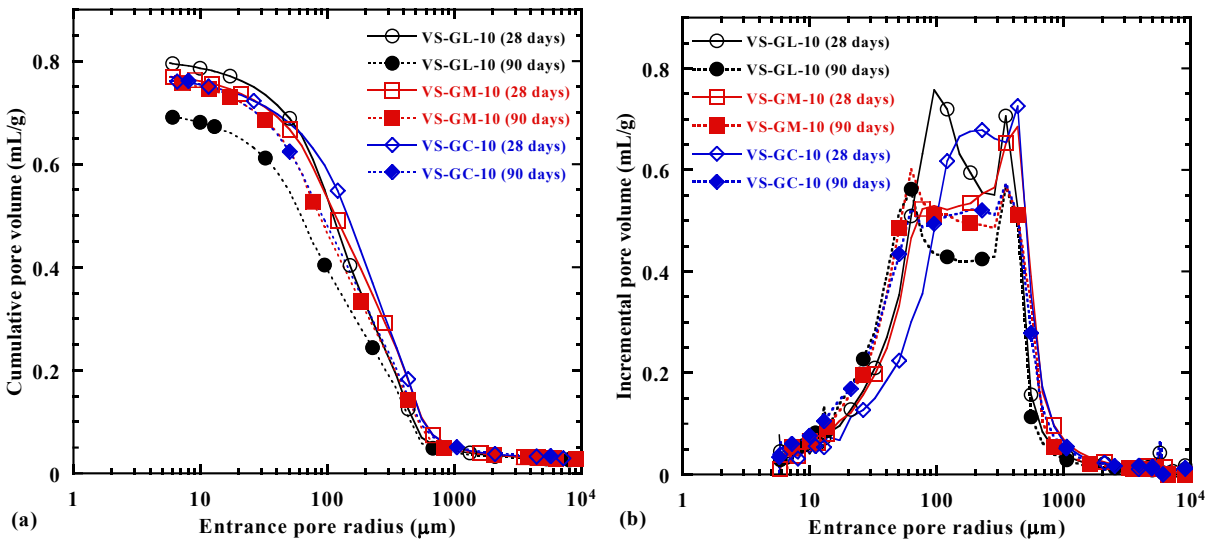

Fig. 13 MIP results for selected stabilized soil at 28 and 90 days (a) mercury intrusion curves and (b) differential pore size distribution

Table 1 Main chemical components of raw materials used in this study

Material	Soil (w_t%)	Cement (w_t%)	GGBS (w_t%)	Lime (w_t%)	Magnesium oxide (w_t%)	Carbide slag (w_t%)
Na_2O	3.54	-	-	-	-	-
MgO	2.45	3.15	8.14	0.93	96.97	1.14
Al_2O_3	18.45	7.45	14.04	0.71	-	1.90
SiO_2	58.14	20.13	32.60	0.21	0.53	23.43
P_2O_5	0.76	-	-	-	-	-
SO_3	0.45	5.55	2.39	0.30	1.42	0.69
K_2O	3.16	1.32	0.46	-	-	0.30
CaO	3.78	63.71	41.42	97.67	1.08	72.31
TiO_2	1.14	0.54	0.65	-	-	0.09
MnO	0.17	-	-	-	-	-
Fe_2O_3	7.96	3.14	0.30	0.18	-	0.14

Note: w_t% refers to the weight percentage.

Table 2 Testing programme

Treatment methods	Case No.	Binder				Vacuum pressure (kPa)
		Cement Content (%)	GGBS content (%)	Activator	Activator content (%)	
vacuum-only **p**reloading	VP	-	-	-	-	-80
binder-only **s**olidification	BS-C	10	-	-	-	-
vacuum-**s**olidification combined	VS-GL-5	-	10	Lime	5	-80
	VS-GL-10	-	10	Lime	10	-80
	VS-GL-20	-	10	Lime	20	-80
	VS-GL-40	-	10	Lime	40	-80
	VS-GM-5	-	10	MgO	5	-80
	VS-GM-10	-	10	MgO	10	-80
	VS-GM-20	-	10	MgO	20	-80
	VS-GM-40	-	10	MgO	40	-80
	VS-GC-10	-	10	CS	10	-80
	VS-GC-20	-	10	CS	20	-80
	VS-C	10	-	-	-	-80

Note: Cement content refers to the mass ratio of cement to dry soil; GGBS content refers to the mass ratio of GGBS to dry soil, and activator content is the mass ratio of activator to GGBD.

Table 3 Comparison of vacuum dewatering performance for cases with alkali-activated GGBS

No.	Activator Type	Activator content (%)	m_{dw} (kg)	t_e (day)	$m_{dw.}$ ratio	t_e ratio
VS-GL-5	Lime	5	15.3	4.2	1.43	1.68
VS-GL-10	Lime	10	15.4	4.2	1.44	1.68
VS-GL-20	Lime	20	13.2	3.2	1.23	1.28
VS-GL-40	Lime	40	14.3	3.0	1.34	1.20
VS-GM-5	MgO	5	14.8	3.7	1.38	1.48
VS-GM-10	MgO	10	15.2	3.7	1.42	1.48
VS-GM-20	MgO	20	14.5	2.7	1.36	1.08
VS-GM-40	MgO	40	14.0	2.6	1.31	1.04
VS-GC-10	CS	10	16.4	4.7	1.53	1.88
VS-GC-20	CS	20	16.1	4.7	1.50	1.88

Note: m_{dw} = the mass of discharged water after vacuum preloading; t_e = the effective time of vacuum dewatering.

13 Table 4 pH of discharged water by vacuum

Case No.	VS-GL-5	VS-GL-10	VS-GL-20	VS-GL-40
pH	9.36	11.53	12.16	12.57
Case No.	VS-GM-5	VS-GM-10	VS-GM-20	VS-GM-40
pH	9.23	9.45	11.59	12.10
Case No.	VS-GC-10	VS-GC-20	VS-C	VP
pH	9.17	11.92	12.32	7.52

14